

1 **Grounding and Calving Cycle of Mertz Ice Tongue**

2 **Revealed by Shallow Mertz Bank**

3 Xianwei Wang^{1,2}, David M. Holland^{2,3}, Xiao Cheng^{1,5} and Peng Gong^{4,5}

4 1. State Key Laboratory of Remote Sensing Science, and College of Global Change and Earth System Science,
5 Beijing Normal University. Beijing 100875, China.

6 2. Center for Global Sea Level Change, New York University Abu Dhabi. Abu Dhabi, United Arab Emirates.

7 3. Courant Institute of Mathematical Sciences, New York University. New York 10012, United States of America.

8 4. Ministry of Education Key Laboratory for Earth System Modeling, and Center for Earth System Science,
9 Tsinghua University, Beijing, China 100084.

10 5. Joint Centre for Global Change Studies, Beijing, China.

11
12 *Correspondence to: wangxianwei0304@163.com*

13 **Abstract**

14 A recent study, using remote sensing, provided some evidence that a seafloor shoal
15 influenced the 2010 calving event of the Mertz Ice Tongue (MIT), by partially grounding the
16 MIT several years earlier. In this paper, we start by proposing a method to calculate Firm Air
17 Content (FAC) around Mertz from seafloor-touching icebergs. Our calculations indicate the FAC
18 around Mertz region as 4.87 ± 1.31 m. We then design an indirect method of using freeboard and
19 sea level data extracted from ICESat/GLAS, FAC, and relatively accurate seafloor topography to
20 detect grounding sections of the MIT between 2002 and 2008 and analyze the process of
21 grounding prior to the calving event. By synthesizing remote sensing data, we point out that the
22 grounding position was localized northeast of the Mertz ice front close to the Mertz Bank. The
23 grounding outlines of the tongue caused by the Mertz Bank are extracted as well. From 2002 to
24 2008, the grounding area increased and the grounding became more pronounced. Additionally,
25 the ice tongue could not effectively climb over the Mertz Bank in following the upstream ice
26 flow direction and that is why MIT rotated clockwise after late 2002. Furthermore, we
27 demonstrate that the area-increasing trend of the MIT changed little after calving ($\sim 36 \text{ km}^2/\text{a}$),
28 thus allowing us to use remote sensing to estimate the elapsed time until the MIT can reground
29 on the shoal. This period is approximately 70 years. The calving of MIT can be cyclical because
30 of the shallow Mertz Bank location and the flow rate of the tongue. The calving cycle of the
31 MIT explains the cycle of sea-surface condition change around the Mertz.

32 **Keywords:** Mertz Ice Tongue, firm air content, iceberg grounding, Mertz Bank, iceberg scouring,
33 calving cycle.

34 **1. Introduction**

35 Surface-warming induced calving or disintegration of floating ice has occurred in
36 Antarctica, such as the Larsen B ice shelf (Scambos et al., 2000, 2003; Domack et al., 2005;
37 Shepherd et al., 2003). While surface or sub-surface melting has largely been recognized to
38 contribute to floating ice loss in Antarctica (Depoorter et al., 2013), calving caused by interaction
39 with the seafloor has not been widely considered. The Mertz Ice Tongue (MIT) was reported to
40 have calved in 2010, subsequent to being rammed by a large iceberg, B-9B (Legresy et al. 2010).
41 After the calving, the areal coverage of the Mertz polynya, and sea-ice production and dense,
42 shelf-water formation in the region changed (Kusahara et al. 2011; Tamura et al. 2012). However,
43 the iceberg collision may have only been an apparent cause of the calving as other factors had
44 not been fully considered such as seafloor interactions (Massom et al., 2015; Wang. 2014). By
45 comparing inverted ice thickness to surrounding bathymetry, and combining remote sensing,
46 Massom et al., (2015) considered that the seabed contact may have held the glacier tongue in
47 place to delay calving by ~8 years. The interaction of the MIT with the seafloor, the exact
48 grounding location of the MIT before calving and how severe the grounding was are still not
49 well-known.

50 The MIT (66°S-68°S, 144°E-150°E, Fig. 1) is located in King George V Land, East
51 Antarctica, with an ice tongue extending over 140 km from its grounding line to the tongue front
52 and approximately 30 km wide at the front (Legresy et al., 2004). Much field exploration has
53 been conducted around Mertz and the increasing availability over the last decade of remote
54 sensing, hydrographic surveying, and bathymetric data allow the causes of ice tongue instability
55 to gradually come into focus. From satellite altimetry, a modest elevation change rate of 0.03 m/a
56 (Pritchard et al., 2012) and a freeboard change rate of -0.06 m/a (Wang et al., 2014) were found,

57 which implied that the combined effects of surface accumulation and basal melt were not
58 dramatic for this ice tongue. For the MIT, investigations of tidal effects, surface velocity, rift
59 propagation, and ice front propagation (Berthier et al., 2003; Frezzotti et al., 1998; Legresy et al.,
60 2004; Lescarmonier et al., 2012; Massom et al., 2010, 2015) have been conducted with an
61 objective of detecting underlying factors affecting stability. Grounding as a potential factor can
62 affect the stability of an ice tongue, as recently pointed out by Massom et al. (2015). However,
63 without highly accurate bathymetric data, it is impossible to carry out such study. Fortunately, In
64 2010, a new and high resolution bathymetry model, for the seafloor surrounding the Mertz, with
65 a resolution of 100 m was released for the Terra Adelie and George V continental margin
66 (Beaman et al., 2011), and incidentally later used to generate the Bedmap-2 (Fretwell et al.,
67 2013). Such accurate data provides an opportunity for better exploring seafloor shoals and their
68 impact on the instability of MIT. In this study, we focus on the grounding event of the MIT from
69 2002 to 2008. A method for grounding event detection is proposed and the grounding of the MIT
70 before calving is investigated. A calving cycle of the MIT caused by grounding is discussed as
71 well.

72 **2. Data**

73 The primary data used to investigate ice tongue grounding in this study are Geoscience
74 Laser Altimeter System (GLAS) data onboard the Ice, Cloud and land Elevation Satellite
75 (ICESat) and the seafloor bathymetry data mentioned above. In this section, ICESat/GLAS and
76 bathymetry data, as well as some preprocessing are introduced.

77 **2.1 ICESat/GLAS**

78 The ICESat is the first spaceborne laser altimetry satellite orbiting the Earth, launched by
79 National Aeronautics and Space Administration (NASA) in 2003 (Zwally et al. 2002) with

80 GLAS as the primary payload onboard. ICESat/GLAS was operated in an orbit of ~600 km and
81 had a geographical coverage from 86° S to 86° N. ICESat/GLAS usually observed in nadir
82 viewing geometry and employed laser pulses of both 532 nm and 1064 nm to measure the
83 distance from the sensor to the ground (Zwally et al. 2002). On the ground, ICESat/GLAS's
84 footprint covered an area of approximately 70 m in diameter, with each adjacent footprints
85 spaced by ~170 m. The horizontal location accuracy of the footprint was about 6 m (Abshire et al.
86 2005). The accuracy and precision of ICESat/GLAS altimetry data were 14 cm and 2 cm
87 respectively (Shuman et al. 2006). ICESat/GLAS usually made two or three campaigns a year
88 from 2003 to the end of 2009, with each campaign lasting for about one month. With billions of
89 laser footprints received by the telescope, 15 types of data were produced for various scientific
90 applications, named as GLA01, GLA02, ... GLA15. In this study, GLA12 data (elevation data
91 for polar ice sheet) covering the Mertz from release 33 during the interval of 2003 to 2009 is
92 used, the spatial distribution of which is shown in Fig. 2.

93 **2.2 Seafloor Topography**

94 Detailed bathymetry maps are fundamental spatial data for marine science studies
95 (Beaman et al., 2003, 2011) and crucially needed in the data-sparse Antarctic coastal region
96 (Massom et al. 2015). Regionally, around Mertz, a large archive of ship track single-beam and
97 multi-beam bathymetry data from 2000 to 2008 were used to generate a high resolution Digital
98 Elevation Model (DEM), the spatial coverage of which can be found in Fig. 2 of Beaman et al.
99 (2011) and bathymetry data coverage over the Mertz region can be found from S-Fig. 1. The
100 DEM product was reported as having a vertical accuracy of about 11.5 m (500 m depth) and
101 horizontal accuracy of about 70 m (500 m depth) in the poorest situation (Beaman et al. 2011).
102 Around Antarctica, seafloor topography data from Bedmap-2 was produced by Fretwell et al.

103 (2013) which adopted the DEM from Beaman et al. (2011). In this study, Bedmap-2 seafloor
104 topography data covering Mertz is employed to detect the contact between seafloor and the MIT.
105 Because of inconsistent elevation systems for ICESat/GLAS and seafloor topography data, the
106 Earth Gravitational Model 2008 (EGM08) geoid with respect to World Geodetic System 1984
107 (WGS-84) ellipsoid is taken as reference. Since seafloor topography from Bedmap-2 is
108 referenced to the so-called g104c geoid, an elevation transformation is required and can be
109 implemented through Eq. (1).

$$110 \quad E_{sf} = E_{seafloor} + gl04c_{to_wgs84} - EGM2008 \quad (1)$$

111 where ' E_{sf} ' and ' $E_{seafloor}$ ' is the seafloor topography under EGM08 and g104c respectively,
112 ' $gl04c_{to_wgs84}$ ' is the value needed to convert height relative to g104c geoid to that under WGS-
113 84, and ' $EGM2008$ ' is the geoid undulation with respect to WGS-84.

114 **3. Methods**

115 **3.1 Grounding Detection Method**

116 ICESat/GLAS data has been widely used to determine ice freeboard, or ice thickness,
117 since its launch in 2003 (Kwok et al., 2007; Wang et al., 2011, 2014; Yi et al., 2011; Zwally et
118 al., 2002, 2008). To study ice freeboard, draft, and grounding of the MIT through time,
119 ICESat/GLAS GLA12 data from release 33 from 2003 to 2009 are used as mentioned, and the
120 spatial coverage of which can be seen in Fig. 2. The methods we designed for grounding
121 detection of the MIT are now introduced. First, assuming a floating ice tongue, based on
122 freeboard data extracted in different observation dates, the ice draft of the MIT is inverted. Next,
123 ice bottom elevation is calculated based on the inverted ice draft and the lowest sea-surface
124 height. Finally, the ice bottom is compared with seafloor bathymetry and ice grounding is

125 detected. The underlying logic for grounding detection is that if the inverted ice bottom is lower
126 than seafloor, we can draw a conclusion that the ice tongue is grounded rather than floating.

127 The method to extract a freeboard map using ICESat/GLAS from multiple campaigns
128 over the MIT was described in Wang et al. (2014). Here, we do not revisit it in detail but
129 introduce it schematically. Four steps are included in freeboard map production for each of
130 November 14, 2002, March 8, 2004, December 27, 2006 and January 31, 2008..

131 The first step is on data preprocessing, saturation correction, data quality control, and
132 tidal correction removal. The magnitude of the ICESat/GLAS waveform can become saturated
133 because of different gain setting, or the occurrence of cloud. Thus the saturated waveforms with
134 '*i_satElevCorr*' (i.e. an attribute from GLA12 data record) greater than or equal to 0.50 m are
135 ignored and those with '*i_satElevCorr*' less than 0.50 m are corrected by adding the correction
136 back (Wang et al. 2012, 2013). Additionally, measurements with '*i_reflectUC*' greater than or
137 equal to one are ignored. Furthermore, tidal correction from TPX07.1 tide model in GLA12 data
138 record is removed to obtain elevation data on the instantaneous sea surface condition. Finally,
139 elevation data under WGS-84 ellipsoid and EGM 08 geoid for ICESat/GLAS from 2003 to 2009
140 is prepared for subsequent use.

141 The second step is to derive sea-level height according to each track and to calculate
142 freeboard for each campaign. Because of tidal variations near the MIT, surface elevations of the
143 MIT can vary as well. To derive sea-level height from ICESat/GLAS and provide a reference for
144 freeboard calculation for different campaigns, ICESat/GLAS data over the MIT within a buffer
145 region (with 10 km as buffer radius of MIT boundary in 2007) are selected and sea-level height
146 is determined as the lowest elevation measurement along each track (Wang et al. 2014).
147 Freeboard is then calculated by subtracting the corresponding sea-level height from elevation

148 measurement of the MIT according to different tracks even in the same campaign. Thus
149 freeboard data for different campaigns from 2003 to 2009 is obtained.

150 The third step is to relocate footprints using estimated ice velocity. ICESat observed the
151 MIT almost repeatedly along the same track in different campaigns (Fig. 2). However,
152 observation from only one campaign cannot provide good coverage of the MIT, which drives us
153 to combine all observations from 2003 to 2009 together to produce a freeboard map of MIT. Fig.
154 2 shows the spatial coverage of ICESat/GLAS from 2003 to 2009 over the Mertz, but the
155 geometric relation between tracks is not correct over the MIT because the tongue was fast
156 moving and observed in different years by the ICESat. The region observed in an earlier
157 campaign would move downstream later (Wang et al. 2014). For example, ICESat collected data
158 from track T31 on March 22, 2003 and T165 (Fig. 2) on November 1, 2003 respectively. Fig. 2
159 shows the distance between track T165 and T31, ~ 7.5 km without considering ice flow. However
160 because of the fast moving ice tongue, the distance of their actual ground tracks on the surface of
161 the MIT should be a little larger because T165 is located upstream and observed later. Thus
162 footprints relocation using ice velocity is critical to obtain accurate geometric relations among
163 different tracks. The ice velocity data from Rignot et al. (2011) generated from InSAR data from
164 2006 to 2010 is used to relocate the footprints of ICESat/GLAS. Thus the correct geospatial
165 relations between observations from different campaigns can be achieved on November 14, 2002,
166 March 8, 2004, December 27, 2006, and January 31, 2008, through Eqs. (2) and (3). The
167 freeboard change with time should be considered as well, but this contribution is neglected
168 because freeboard comparison from crossing tracks showed a slightly decreasing trend of -0.06
169 m/a on average (Wang et al. 2014). The spatial distribution of freeboard data over the MIT
170 corresponding to November 14, 2002, is shown in Fig. 5(a).

171
$$X = x + \sum_{i=1}^n v_{xi}\Delta t + v_{xm}t_m \quad (2)$$

172
$$Y = y + \sum_{i=1}^n v_{yi}\Delta t + v_{ym}t_m \quad (t_m = t_2 - t_1 - n\Delta t) \quad (3)$$

173 where ‘ x ’ and ‘ y ’ is location in the X and Y directions from ICESat measurement directly;
 174 ‘ X ’ and ‘ Y ’ is location in the X and Y directions after relocation; ‘ v_x ’ and ‘ v_y ’ is the ice velocity
 175 in the X and Y directions respectively; ‘ t_1 ’ and ‘ t_2 ’ is the start and end time; ‘ Δt ’ is the time
 176 interval and ‘ n ’ indicates the largest integer time steps for time interval between ‘ t_1 ’ and ‘ t_2 ’;
 177 ‘ t_m ’ is the residual time; In this work, ‘ Δt ’ is set as 10 days; ‘ v_{xi} ’ and ‘ v_{yi} ’ is derived from ice
 178 velocity field according to different locations during relocation and may change in different time
 179 intervals.

180 The forth step is to interpolate the freeboard map using the relocated freeboard data from
 181 step three. Inverse Distance Weighting, Natural Neighbor, Spline and Kriging are most widely
 182 used interpolation techniques (Childs. 2004). Kriging interpolation under spatial analysis toolbox
 183 of ArcGIS is selected in this study to produce freeboard maps of the MIT because kriging can
 184 provide an optimal interpolation estimate for a given coordinate location by considering the
 185 spatial relationships of a data set. . With this method, freeboard maps of the MIT are produced on
 186 November 14, 2002, March 8, 2004, December 27, 2006, and January 31, 2008, because of
 187 known ice tongue outlines from Landsat images.

188 Ice draft is calculated with Eq. (4) assuming hydrostatic equilibrium and the lowest sea-
 189 surface height (further discussed later in Section 6.2.2) is extracted as well from ICESat/GLAS
 190 data from all campaigns covering this region, which was -3.35 m under EGM 08 (WGS-84). For
 191 time varying sea-surface heights caused by tides, the minimum sea-surface height can allow ice
 192 with a given draft to ground to the seafloor. Then, ice bottom elevation is calculated by
 193 considering the ice draft and the lowest sea-surface height. To compare the ice bottom with the

194 seafloor, an elevation difference of both is calculated. In this way, a negative value indicates that
195 ice bottom is lower than seafloor, which corresponds to grounding.

$$196 \rho_w D = \rho_i (H_f + D - FAC) \quad (4)$$

197 where ‘ D ’ is ice draft, i.e. vertical distance from sea surface to bottom of ice; ‘ H_f ’ is freeboard,
198 i.e. vertical distance from sea surface to top of snow; ‘ ρ_w ’ and ‘ ρ_i ’ are densities of ocean water
199 and ice, respectively. In this study, ice and sea water density are taken as 915 kg/m^3 and 1024
200 kg/m^3 , respectively (Wang et al., 2014); ‘ FAC ’ is the firm air content, the decrease in thickness
201 (in meters) that occurs when the firm column is compressed to the density of glacier ice, as
202 defined in Holland et al., (2011) and Ligtenberg et al. (2014). The calculation of firm air content
203 around Mertz will be soon introduced in Section 3.2. In this work, we define the elevation of at
204 the underside (bottom) of the tongue as ‘ E_{ice_bottom} ’ and is calculated by Eq. (5).

$$205 E_{ice_bottom} = E_{sea_level} - D \quad (5)$$

206 where ‘ E_{ice_bottom} ’ corresponds to elevation of the ice bottom. ‘ E_{sea_level} ’ is the lowest sea-
207 surface height among extracted sea-surface height from different tracks and different campaigns,
208 which is -3.35 m . Similarly, the elevation difference of ice tongue bottom and seafloor is defined
209 as ‘ E_{dif} ’, which can be calculated by Eq. (6).

$$210 E_{dif} = E_{ice_bottom} - E_{sf} \quad (6)$$

211 where ‘ E_{dif} ’ is elevation difference by subtracting the seafloor elevation from the ice bottom.

212 **3.2. Firm Air Content Estimation Method**

213 The Antarctic ice sheet is covered by a dry, thick firm layer which represents an
214 intermediate stage between fresh snow and glacial ice, having varying density from Antarctic
215 inland to the coast (Van den Broke, 2008). The density and depth of the Antarctic firm layer has
216 been modeled (e.g., Van den Broke, 2008) using a combination of regional climate model output

217 and a steady-state firn compaction model. However, for ice thickness inversion, Firn Air Content
218 (FAC) is usually used to make the calculation convenient (Rignot and Jacobs. 2002), defined as
219 the decrease in thickness (in meters) that occurs when the firn column is compressed to the
220 density of glacier ice (Holland et al., 2011). Time-dependent FAC has also been modeled by
221 considering the physical process of the firn layer (e.g., Ligtenberg et al. 2014). For the MIT,
222 there are some in-situ measurements of snow thickness available from Massom et al. (2010) who
223 used a snow layer depth of 1 m to derive the thickness of surrounding multi-year, fast sea ice.
224 However on the surface of the MIT, no in-situ measurements of density or depth of firn layer are
225 available.

226 Because of different density and thickness of the firn layer on top layer of an ice tongue,
227 it is challenging to simulate the density profile of the MIT without in-situ measurements as
228 control points. In this study, we use FAC extracted from adjacent seafloor-touching icebergs to
229 investigate the grounding of the MIT rather than FAC from modeling. MIT may be composed of
230 pure ice, water, air, firn or snow that makes ice mass calculation complicated. However, if
231 assuming a pure ice density only to calculate ice mass, the thickness of MIT must be corrected
232 by FAC. FAC correction to ice thickness can be inferred from surrounding icebergs calving from
233 MIT using Eq. (4) when knowing ice draft and freeboard assuming hydrostatic equilibrium.
234 Thus one critical issue is to target and use icebergs fulfilling these requirements to solve Eq. (4),
235 such as slightly grounded icebergs above already known seafloor with observed freeboard. From
236 Smith (2011), icebergs can be divided into three categories based on bathymetry and seasonal
237 pack ice distributions: grounded, constrained, and free-drifting icebergs. Without occurrence of
238 pack ice, an iceberg can be free-drifting or grounded. Free-drifting icebergs can move several
239 tens of kilometers per day, such as iceberg A-52 (Smith et al. 2007). Grounded icebergs can be

240 firmly or lightly anchored. Heavily grounded icebergs have firm contact with the seafloor and
241 can be stationary for a long time, such as iceberg B-9B (Massom. 2003). However, slightly
242 grounded icebergs may have little contact with the seafloor and can possibly move slowly under
243 the influence of ocean tide, ocean currents, or winds, but much slower than free-drifting icebergs.
244 The relation of grounded and ice drifting velocity is not well-known. However, from slowly
245 drifting or nearly stationary icebergs in open water, we can determine if an iceberg is grounded.

246 Because of the heavily grounded iceberg B-9B to the east of the MIT blocking the
247 drifting of pack ice or icebergs from the east, icebergs located between B-9B and the MIT are
248 most likely generated from the Mertz or Ninnis glaciers. We calculate the FAC from these
249 icebergs and later apply it to grounding event detection of the MIT, in terms of estimating the
250 FAC of the MIT itself. Around the MIT, the locations of three icebergs ('A', 'B' and 'C') were
251 identified using MODIS and Landsat images in austral summer, 2006 and 2008 and shown in Fig.
252 4. Fortunately, ICESat/GLAS observed these icebergs on February 23, 2006 (54th day of 2006)
253 and February 18, 2008 (49th day of 2008). This allows us to analyze the behavior of the icebergs
254 three-dimensionally. From Fig. 4a, icebergs 'A', 'B' and 'C' changed position little in about two
255 months (from 28 to 85 day of 2006). Thus we can consider these icebergs slightly grounded.
256 These slightly grounded icebergs may plough the seafloor and leave ridges or grooves. In Pine
257 Island Trough, ridges on the seafloor have been already found with a range of 1 to 2 m, which
258 was believed to be influenced by grounding icebergs drifting with tides (Jakobsson et al. 2011;
259 Woodworth-Lynas et al. 1991). From this viewpoint, we are confident that under the lowest sea
260 level (lowest tide), these iceberg must be grounded, which means that the ice draft inverted from
261 freeboard measurement assuming hydrostatic equilibrium must be greater than or equal to water
262 depth. Based on this analysis, we can take water depth as draft to calculate the FAC.

263 Because only ‘A’ and ‘C’ were observed by track T1289 of the ICESat/GLAS in 2006,
264 freeboard and water depth from bathymetry for both are used to calculate the FAC (Fig. 4, 9 and
265 Table 1). However, the icebergs were not stationary, which indicates only some parts were
266 grounded. In this study, only the top two largest freeboard measurements of icebergs ‘A’ and ‘C’
267 from T1289 in 2006 are employed to calculate the FAC with Eq. (7) with a least-squares method
268 under hydrostatic equilibrium.

$$269 \quad FAC = H_{f_k} + D_k - \frac{\rho_w}{\rho_i} D_k + \varepsilon_k \quad (7)$$

270 where ‘*k*’ is used to identify different icebergs ‘A’ or ‘C’, ‘*H_f*’ is the top two largest freeboard
271 measurement of each iceberg, ‘*D*’ is ice draft which is the same as sea water depth and is taken
272 from seafloor bathymetry directly, ‘ ε ’ is a residual for FAC.

273 Table 1 shows the freeboard and seafloor bathymetry under the icebergs in 2006 for FAC
274 calculation and grounding detection of icebergs in 2008 (detailed freeboard values for these
275 icebergs can be seen from Fig. 9). With freeboard and seafloor measurements from iceberg ‘A’
276 and ‘C’ in 2006 (Table 1), the FAC is calculated as about 4.87 ± 1.31 m. Two icebergs ‘A’ and ‘B’
277 were observed by the same track T1289 of the ICESat/GLAS on February 18, 2008 and thus are
278 used to evaluate the grounding detection using this FAC. From iceberg trajectories observed by
279 remote sensing (Fig. 4b), we know, iceberg ‘A’ drifted away from its original position. Thus it
280 was not grounded. However, iceberg ‘B’ kept rotating in this period without drifting away, from
281 which we can consider it grounded. Such grounding status determined from remote sensing can
282 also be detected with our method since the elevation difference of ice bottom and seafloor from
283 Table 1 does clearly indicate a grounded iceberg ‘B’ and a floating iceberg ‘A’. Thus, our FAC
284 estimation works well around Mertz.

285 **4. Accuracy of Grounding Detection**

286 The accuracy of ‘ E_{dif} ’ is critical to grounding detection of the MIT. From Eq. (1) to (6),
 287 we find different components of the error sources, such as from sea surface height
 288 determination, ice draft, seafloor bathymetry, and elevation transformation. Meanwhile,
 289 uncertainty of ice draft is primarily determined by that of freeboard and ‘ FAC ’. Furthermore, the
 290 uncertainty of freeboard is influenced by footprint relocation and freeboard changing rates.
 291 Considering all mentioned above, the error source of elevation difference ‘ E_{dif} ’ can be
 292 synthesized by Eq. (8):

$$293 \quad \Delta E_{dif} = \Delta E_{sl} + a(\Delta H_f + \Delta E_{re} + \Delta E_{fb_c} + \Delta FAC + \Delta E_{krig}) + \Delta E_{sf} + \Delta E_{trans} \quad (8)$$

294 where $a = \frac{\rho_i}{\rho_w - \rho_i}$; ‘ Δ ’ stands for error of each variable; ‘ ΔE_{dif} ’ stands for error of final elevation
 295 difference of ice bottom and seafloor; ‘ ΔE_{sl} ’, ‘ ΔH_f ’, ‘ ΔE_{re} ’, ‘ ΔE_{fb_c} ’, ‘ ΔFAC ’, ‘ ΔE_{sf} ’ and
 296 ‘ ΔE_{krig} ’, ‘ ΔE_{trans} ’ stand for errors caused by sea surface height extraction, freeboard extraction,
 297 freeboard relocation, freeboard changing rates, FAC calculation, seafloor bathymetry, kriging
 298 interpolation and elevation system transformation, respectively.

299 Usually, the influence of elevation system transformation on final elevation difference
 300 can be neglected. Based on the error propagation law, the uncertainty of elevation difference
 301 ‘ E_{dif} ’ can be described by Eq. (9):

$$302 \quad \varepsilon E_{dif} = \sqrt{(\varepsilon E_{sl})^2 + a^2[(\varepsilon H_f)^2 + (\varepsilon E_{re})^2 + (\varepsilon E_{fb_c})^2 + (\varepsilon FAC)^2 + (\varepsilon E_{krig})^2]} + (\varepsilon E_{sf})^2 \quad (9)$$

303 where ‘ ε ’ indicates the uncertainty of each parameter.

304 **4.1 Uncertainty of kriging interpolation**

305 Fig. 5a shows the spatial distribution of freeboard data over the MIT used for detecting
 306 grounding on November 14, 2002. The spatial difference of ICESat/GLAS between Fig. 2 and

307 Fig. 5 are caused by footprint relocation, after which the spatial geometry between different
308 tracks is relatively correct. In the lower right of the Mertz ice front (Fig. 5a), the freeboard
309 distance between track T1289 and T165 is about 7 km. In these data gaps, freeboard data used
310 for grounding detection in Section 3.1 is interpolated using kriging. Thus, knowing the
311 uncertainty of kriging interpolation is critical to final grounding detection.

312 To investigate interpolation uncertainty of the kriging method, freeboard measurements
313 should be compared with interpolation ones. Thus, a testing region with freeboard measurements
314 is selected, indicated by a blue dashed square in Fig. 5a, about 7 km×7 km. A freeboard map is
315 first interpolated with gray dots only (Fig. 5a) using kriging. Then, the freeboard measurements
316 (284 of green dots in Fig. 5a) are compared with interpolation in the square. The spatial
317 distribution and the histogram of freeboard difference derived by subtracting krigged freeboard
318 from freeboard derived from ICESat/GLAS is shown in Fig. 5b.

319 In this square, the freeboard measurement varies from 31.6 m to 40.0 m with 36.6 m as
320 the average. However, the freeboard interpolation varies from 32.9 m to 39.6 m with 35.9 m as
321 the average. From the freeboard difference results (Fig. 5b), we find that the interpolation results
322 show similar results compared with freeboard derived from ICESat/GLAS. The interpolated
323 freeboard has an accuracy of -0.7 ± 1.8 m. The interpolated freeboard using kriging can reflect
324 the actual freeboard well. Also, the distribution of freeboard difference in Fig. 5b does not show
325 obvious geospatial variation trend.

326 **4.2 Grounding Detection Robustness**

327 Since sea level is extracted from ICESat/GLAS data track by track, we use ± 0.15 m as
328 the uncertainty of elevation data (εE_{sl}). Also from Wang et al. (2014), we can see the
329 uncertainty of freeboard extraction (εH_f) is ± 0.50 m. From Rignot et al. (2011), the error of ice

330 velocity ranged from 5 m/a to 17 m/a. Assuming that ice velocity varied by 17 m/a (an upper
331 threshold), the relocation error horizontally could reach ± 54 m in an average of three years.
332 Wang et al. (2014) extracted the average slope of the MIT along ice flow direction as 0.00024.
333 However, because of large crevasses on the surface, we use 50 times of this value as a
334 conservative estimate of the average slope. In this way, we can estimate ' εE_{re} ' as ± 0.65 m when
335 considering a three-year period. The annual rate of freeboard change from 2003 to 2009 is -0.06
336 m/a (Wang et al. 2014). Therefore, we consider the freeboard stable over this period. However,
337 when combining data from different time periods then ' εE_{fb_c} ' is estimated as about ± 0.18 m if
338 considering three years time difference. From Beaman et al. (2011), considering elevation
339 uncertainty at the worst situation when water depth is 500 m, ' εE_{g104c} ' is ± 11.5 m. For kriging
340 interpolation, from analysis in Section 4.1, 1.8 m is taken as the uncertainty. Using all these
341 errors above, we calculate the final uncertainty of elevation difference as ± 23 m.

342 From the calculations above, we can say that ' E_{dif} ' less than 23 m corresponds to a very
343 robust grounding event. However, if the ' E_{dif} ' is greater than 23 m, we can not confirm
344 grounding. ' E_{dif} ' in the interval of -23m to 23 m corresponds to slight grounding or floating.
345 We can also determine different contributions of each separate factor to the overall accuracy.
346 Seafloor bathymetry contributes the largest part and is the dominant factor affecting the accuracy
347 of grounding detection.

348 **5. Grounding Detection Results**

349 The spatial distribution of elevation difference ' E_{dif} ' and outline of the MIT from 2002
350 to 2008 is shown in Fig. 6. A buffer region with radius of 2 km (region between black and grey
351 lines in Fig. 6) is introduced to investigate grounding potential of the MIT, if it approached there.
352 The elevation difference less than 46 m (twice of elevation difference uncertainty ' εE_{dif} ') both

353 inside and outside of the outline is extracted and the corresponding statistics are shown in Table
354 2. Since the uncertainty to determine a grounding event is about $\pm 23\text{m}$, if some grid points of the
355 MIT have elevation difference ' E_{dif} ' less than 23 m, we can conclude that this section of the
356 tongue is almost grounded. The smaller the ' E_{dif} ', the more robust the grounding. From the
357 color-change patterns of Fig. 6a-d, we can see that part of the ice front grounded on the shallow
358 Mertz Bank from the end of 2002.

359 As illustrated from Table 2, the minimum ' E_{dif} ' inside of the MIT are all less than 23 m
360 and the mean and minimum of the ' E_{dif} ' in the buffer region are all less than 0 from 2002 to
361 2008. From this, we conclude that the ice tongue has grounded on the shallow Mertz Bank since
362 November 14, 2002. This result coincides with findings from Massom et al. (2015) who
363 considered that the northwestern extremity of the MIT started to contact with the seafloor shoal
364 in late 2002 to early 2003. Also it would be hard for the MIT to approach the buffer region
365 (indicated with yellow to red color in Fig. 6) as the surrounding Mertz Bank gets shallower and
366 steeper and substantive grounding would happen if it moved into these regions. Inside of the
367 MIT, the minimum of elevation difference was just 11.9 m on November 14, 2002, which
368 indicates little to no grounding. However on March 8, 2004, December 27, 2006, and January 31,
369 2008, the minimum of elevation difference reached -46.0 m, -52.3 m and -34.8m respectively,
370 which means significant grounding occurred in some regions. From 2002 to 2008, more regions
371 under the MIT have ' E_{dif} ' less than 46 m, the area of which increased from 8 km² to 17 km².
372 Additionally, the mean of ' E_{dif} ' under of the tongue for those having ' E_{dif} ' less than 46 m
373 gradually decreases from 28.8 m to 12.3m, according to which we can conclude that the ice front
374 was grounded more significantly with passing time. Additionally, since the grounding area
375 increased from 8 km² to 17 km² (Table 2) and the mean of ' E_{dif} ' decreased from 2002 to 2008,

376 we can say that over the period from 2002 to 2008, the grounding of the northwest flank of the
377 MIT became more widespread.

378 Based on the calculated elevation difference, the grounding outlines of the MIT are
379 delineated for November 14, 2002, March 8, 2004, December 27, 2006 and January 31, 2008,
380 (Fig. 7). For the grounding part of the outline in different years, starting and ending location and
381 perimeter are also extracted, from which we can conclude that the length of the grounding
382 outline of the Mertz Bank is only limited to a few kilometers (Table 3).

383 We find that the lower right (northwest) of the MIT was always grounded and that
384 grounding did not occur in other regions (Fig. 6). The shallowest seafloor elevation the ice front
385 touched was ~ -290 m in November 2002. In 2004, 2006, and 2008, the lower right (northwest)
386 of the MIT even approached the contour of -220 m. Fig. 7 also shows the extension line of west
387 flank in November, 2002, from which we can see that if the ice tongue moved along the former
388 direction, the ice flow would be seriously blocked when approaching the Mertz Bank. The
389 shallowest region of the Mertz Bank has an elevation of about -140 m and the MIT would have
390 needed to climb over this 140 m obstacle to cross past it. The shallow Mertz Bank would have
391 caused grounding during the climbing. This special feature of seafloor shoal facing the MIT can
392 further explain why the ice velocity differed along the east and west flanks of the MIT before
393 calving and why the ice tongue moved clockwise to the east, as pointed out by Massom et al.
394 (2015). However, because of sparsely-distributed bathymetry data (point measurements) in
395 Mertz region used in Massom et al. (2015), this effect could not be easily seen. Here, from our
396 grounding detection results and surrounding high-accuracy bathymetry data, this effect is more
397 clearly observed.

398 **6. Discussion**

399 6.1 Area Changing Rate and ~70-year Calving Cycle of MIT

400 Using Landsat TM/ETM+ images from 1989 to 2013, outlines of the MIT are extracted
401 manually. Assuming a fixed grounding line position over this period, the area of the MIT over
402 this period is calculated. Using these data, from 1989 to 2007, an increasing area rate of the MIT
403 is shown (from 5453 km² to 6126 km²) in Fig. 8. However, the area of the MIT was almost
404 constant from 2007 to 2010, before calving. The largest area of the MIT was 6113 km² closest to
405 the calving event in 2010. After the calving, the area decreased to 3617 km² in November 2010.

406 The rate of area change for the MIT from 1989 to 2007 is also obtained using a least-
407 squares method, corresponding to 35.3 km²/a. However, after the calving a slight higher area-
408 increasing trend of 36.9 km²/a, is found (Fig. 7). On average, the area-increasing rate of the MIT
409 was 36 km²/a.

410 The surface behavior such as ice flow direction changes and middle rift changes caused
411 by grounding was analyzed by Massom et al. (2015). In the history of the MIT, one or two large
412 calving events were suspected to have happened between 1912 and 1956 (Frezzotti et al., 1998)
413 and we consider it likely to be only once because of the influence of the shallow Mertz Bank.
414 When the ice tongue touched the bank, the bank started to affect the stability of the tongue by
415 bending the ice tongue clockwise to the east, as can be seen from velocity changes from Massom
416 et al. (2015). With continuous momentum and flux input from upstream, a large rift from the
417 west flank of the tongue would ultimately have to occur and could potentially calve the tongue.
418 A sudden length shortening of the tongue can be caused by such ice tongue calving as indeed had
419 happened in February, 2010. We also consider that even without a sudden collision of iceberg B-
420 9B in 2010, the ice tongue would eventually calve because of existence of the shallow Mertz
421 Bank.

422 If we take 6127 km² as the maximum area of the MIT, assuming a constant area-changing
423 rate of about 36.9 km²/a after 2010, it will take about 68 years to calve again. When assuming an
424 area changing rate of about 35.3 km²/a as before 2010, it will take a little longer, about 71 years.
425 Therefore, without considering accidental event such as collision with other large icebergs, the
426 MIT is predicted to calve again in ~70 years. Because of the continuous ice flow upstream, the
427 special location and relatively lower depth of the Mertz Bank, the calving is likely repeatable and
428 a cycle therefore exists.

429 After the MIT calved in February, 2010, Mertz polynya size, sea-ice production, sea-ice
430 coverage and high-salinity shelf water formation changed. A sea-ice production decrease of
431 about 14-20% was found by Tamura et al. (2012) using satellite data and high-salinity shelf
432 water export was reported to reduce up to 23% using a state-of-the-art ice-ocean model
433 (Kusahara et al. 2010). Recently, Campagne et al. (2015) pointed out a ~70-year cycle of surface
434 ocean condition and high-salinity shelf water production around Mertz through analyzing
435 reconstructed sea ice and ocean data over the last 250 years. They also mentioned that this cycle
436 was closely related to presence and activity of Mertz polynya. However, the reason for this cycle
437 was not fully understood.

438 From these findings addressed above and MIT calving cycle we found, our explanation is
439 that the calving cycle of the MIT leads to the ~70-year cycle of surface ocean condition and
440 high-salinity shelf water production around Mertz. Calving decreases the length of the MIT
441 suddenly. Then, a short ice tongue reduces the size of Mertz Polynya formed by Antarctic
442 katabatic winds, resulting in lower sea-ice production and further lessens high-salinity shelf
443 water production. Therefore, the cycle of ocean conditions around Mertz found by Campagne et
444 al. (2015) is likely dominated by the calving of the MIT. Additionally, the cycles of MIT calving

445 and surface ocean condition around Mertz coincides with each other well, ~70 years, which
446 make the explanation much more compelling.

447 **6.2 Key issues influencing grounding detection**

448 Several issues on grounding detection require further clarification, such as sea surface
449 height, FAC value and accuracy of seafloor DEM. In this section, their influences on final
450 grounding detection results are more deeply discussed.

451 **6.2.1 The Lowest Sea-Level Extraction**

452 In Section 3.1, the lowest sea level -3.35 m is derived by comparing all sea-surface
453 heights derived from different tracks and campaigns from 2003 to 2009. This constant stands for
454 the lowest sea level from results around Mertz from 2003 to 2009 and is directly from
455 ICESat/GLAS observation. However, because of limited observations in each year,
456 ICESat/GLAS may not catch the lowest one. Sea level lower than -3.35 m may exist over Mertz
457 region which would make the grounding results more severe with occurrence of more negative
458 values in Fig. 6.

459 **6.2.2 Firn Air Content Calculation**

460 FAC varies across the Antarctica ice sheet, usually decreasing from the interior to the
461 coast. In Section 3.2, FAC over Mertz region is derived as 4.87 ± 1.31 m. However from time-
462 dependent FAC modeling results, around Mertz region, FAC is closed to 5-10 meter (Ligtenberg
463 et al. 2014). Our result is smaller. Since there are no in-situ measurements available for
464 verification, further comparison work needs to be conducted. However, this FAC value is
465 derived according to our best knowledge over Mertz and is affected by iceberg status (using our
466 approach) and the maximum freeboard used.

467 First, for FAC calculation, icebergs just touching the seafloor should be used in which
468 case the FAC calculated assuming hydrostatic equilibrium is the same as the actual value.
469 However, it is difficult to ascertain whether an iceberg is just touching the seafloor from remote
470 sensing images. The near stationary or slowly rotating iceberg detected with remote sensing
471 should be grounded more severely than just touching the seafloor, which may result in a
472 calculated FAC theoretically larger than the actual value. Thus, using this FAC result to detect
473 grounding can potentially lead to smaller grounding results. However, once an iceberg or ice
474 tongue is detected as grounded, the result is more convincing.

475 Second, because ICESat/GLAS worked only several times a year on repeat tracks and
476 icebergs was rotating slowly, elevation profile in 2006 and 2008 along the same track T1289
477 may not come from the same ground surface. Fig. 9 shows the freeboard over iceberg ‘A’, ‘B’
478 and ‘C’ derived from ICESat/GLAS from 2006 and 2008. By comparing freeboard of iceberg ‘A’
479 in 2006 (Fig. 9a), and 2008 (Fig. 9c), we can find that the maximum freeboard was larger and the
480 freeboard profile was longer in 2006. Comparatively, the smaller freeboard in 2008 may be
481 caused by ice basal melting or observing different portion of iceberg ‘A’. Since larger freeboard
482 measured in 2006 indicating a high possibility of capturing the thickest portion, the freeboard
483 measurement in 2006 is used to invert the FAC. Additionally, iceberg ‘A’ and ‘C’ did show the
484 similar maximum freeboard (Table 1), which is another important reason for us to choose
485 measurement in 2006 to invert.

486 **6.2.3 Seafloor DEM**

487 High accuracy seafloor elevation is critical to final success of grounding detection. As
488 can be seen from S-Fig.1, there is no bathymetry data under the MIT, which may result in large
489 uncertainty for seafloor interpolation. The oldest bathymetry data collected along margin of the

490 MIT was at least from 2000 (Beaman et al. 2011). Thus, the boundary of the MIT in 2000 is used
491 to identify bathymetry measurement gaps, as is indicated in Fig. 6. But around the Mertz Ice
492 front, both east and west flanks, bathymetry data does exist, which provides control points for
493 seafloor interpolation under the tongue. Since the ice front has a width of ~34 km (Wang et al.
494 2014), the accuracy of seafloor DEM under the MIT varies according to different distances to the
495 control points. Inside of the MIT boundary of 2000, the closer to the white polygon, the better
496 the accuracy the seafloor DEM. Outside of that boundary, the quality of the seafloor DEM data is
497 much better because of the high density of single-beam or multi-beam bathymetry measurements.

498 However, from Beaman et al. (2011), no uncertainty on the seafloor DEM was
499 systematically provided, but only the poorest accuracy of single or multi-beam bathymetric
500 measurements. Since no new bathymetry data is publicly available in this region, further work on
501 evaluation of the seafloor bathymetry is not possible to conduct and interpolation error from
502 kriging using bathymetry data is difficult to supply. Thus, the accuracy under poorest situation
503 for bathymetry data is used, the same as used in Beaman et al. (2011).

504 Since Beaman et al. (2011) provided the most accurate seafloor DEM over Mertz
505 according to our best knowledge, seafloor DEM under the MIT is kept and the grounding
506 detection is conducted as well. Additionally, the ice tongue never stopped flowing further into
507 the ocean, where the bathymetry measurements density is good. From results shown in Fig. 6 all
508 grounding sections of MIT boundary are located outside of the 2000 boundary. Thus the analysis
509 of grounding detection near ice front in 2002, 2004, 2006, and 2008 is convincing. Inside of the
510 2000 boundary, most of the grounding detection results are above 100 m, indicating a floating
511 status of the corresponding ice. Only abnormal seafloor features higher than this seafloor DEM
512 by about 100 m can result in wide grounding inside. Additionally, from surface features of the

513 MIT from Landsat TM/ETM+ images, no abrupt sunlight shadow related to grounding is
514 detected from 1989 to 2010 near the front, which indicates that the judgment of floating ice
515 tongue inside of the 2000 boundary from Fig. 6 is correct. Actually, no matter whether the MIT
516 inside of the 2000 boundary was grounded or not, gradually grounding on the shallow Mertz
517 Bank of the MIT since late 2002 is a fact, which is direct evidence for us to infer the primary
518 cause of the instability of the MIT.

519 **7. Conclusion**

520 In this study, a method of FAC calculation from seafloor-touching icebergs around Mertz
521 region is presented as an important element of understanding MIT grounding. The FAC around
522 the Mertz is about 4.87 ± 1.31 m. This FAC is used to calculate ice draft based on sea level and
523 freeboard extracted from ICESat/GLAS and appears to work well. A method to extract
524 grounding sections of the MIT is described based on comparing inverted ice draft assuming
525 hydrostatic equilibrium with seafloor bathymetry. The final grounding results explain the surface
526 behavior of the MIT. Previous work by Massom et al. (2015) has also provided some evidence
527 for seafloor interaction, in showing that the MIT front had an approximate 280 m draft with the
528 nearby seafloor as shallow as 285 m, suggesting the possibility of grounding. In our work, we
529 have provided ample detailed bathymetry and ice draft calculations. Specifically, ice bottom
530 elevation is inverted using ICESat/GLAS data and compared with seafloor bathymetry during
531 2002, 2004, 2006, and 2008. From those calculations we show conclusively that the MIT was
532 indeed grounded along a specific portion of its northwest flank over a limited region. We also
533 point out that even without collision by iceberg B-9B in early 2010 the ice tongue would
534 eventually have calved because of momentum and flux input from the upstream glacier flow
535 being increasingly opposed by a reaction force from the shoal of the Mertz Bank.

536 From remote sensing images we are able to quantify the rate of increase of area of the
537 MIT before and after the 2010 calving. While the area-increasing trend of the MIT after calving
538 is slightly larger than before, we use the averaged rate to estimate a timescale required for the
539 MIT to re-advance to the area of the shoaling bathymetry from its retreated, calved position. Our
540 estimate is ~70-years, which is remarkably consistent with Campagne et al. (2015) who found a
541 similar period of sea surface changes using seafloor sediment data. A novel point we bring out in
542 our study is that it is the shoaling of the seafloor combined with the rate of advance of the MIT
543 that leads to the 70-year repeat cycle. Also the calving cycle of the MIT explains the observed
544 cycle of sea surface conditions change well, which indicates the calving of the MIT is dominant
545 factor for sea-surface condition change. Understanding the mechanism underlying the periodicity
546 of MIT calving is important as the presence or absence of the MIT has a profound impact on sea
547 ice and hence of bottom water formation in the local region.

548 **Acknowledgements**

549 This research was supported by Fundamental Research Fund for the Central University,
550 the Center for Global Sea Level Change (CSLC) of NYU Abu Dhabi (Grant: G1204), the Open
551 Fund of State Key Laboratory of Remote Sensing Science (Grant: OFSLRSS201414), and the
552 China Postdoctoral Science Foundation (Grant: 2012M520185, 2013T60077). We are grateful to
553 the Chinese Arctic and Antarctic Administration, the European Space Agency for free data
554 supply under project C1F.18243, the National Snow and Ice Data Center (NSIDC) for the
555 availability of the ICESat/GLAS data (<http://nsidc.org/data/order/icesat-glas-subsetter>) and
556 MODIS image archive over the Mertz glacier ([http://nsidc.org/cgi-](http://nsidc.org/cgi-bin/modis_iceshelf_archive.pl)
557 [bin/modis_iceshelf_archive.pl](http://nsidc.org/cgi-bin/modis_iceshelf_archive.pl)), British Antarctica Survey for providing Bedmap-2 seafloor
558 topography data (<https://secure.antarctica.ac.uk/data/bedmap2/>), the National Geospatial-

559 Intelligence Agency for publicly released EGM2008 GIS data (<http://earth->
560 info.nga.mil/GandG/wgs84/gravitymod/egm2008/egm08_gis.html), and the USGS for Landsat
561 data (<http://glovis.usgs.gov/>). Fruitful discussions with M. Depoorter, P. Morin, T. Scambos and
562 R. Warner, and constructive suggestions from Editor Andreas Vieli and two anonymous
563 reviewers are acknowledged.

564 **References**

- 565 1. Beaman, R. J., & Harris, P. T. (2003). Seafloor morphology and acoustic facies of the
566 George V Land shelf. *Deep Sea Research Part II: Topical Studies in Oceanography*,
567 50(8), 1343-1355.
- 568 2. Beaman, R. J., O'Brien, P. E., Post, A. L., & De Santis, L. (2011). A new high-resolution
569 bathymetry model for the Terre Adélie and George V continental margin, East Antarctica.
570 *Antarctic Science*, 23(01), 95-103.
- 571 3. Berthier, E., Raup, B., & Scambos, T. (2003). New velocity map and mass-balance
572 estimate of Mertz Glacier, East Antarctica, derived from Landsat sequential imagery.
573 *Journal of Glaciology*, 49(167), 503-511.
- 574 4. Ballantyne, J., 2002. A multidecadal study of the number of Antarctic icebergs using
575 scatterometer data. Brigham Young University online report:
576 [〈http://www.scp.byu.edu/data/iceberg/IcebergReport.pdf〉](http://www.scp.byu.edu/data/iceberg/IcebergReport.pdf) .
- 577 5. Campagne, P., Crosta, X., Houssais, M. N., Swingedouw, D., Schmidt, S., Martin, A., ...
578 & Massé G. (2015). Glacial ice and atmospheric forcing on the Mertz Glacier Polynya
579 over the past 250 years. *Nature Communications*, 6.
- 580 6. Childs, C. (2004). Interpolating surfaces in ArcGIS spatial analyst. *ArcUser*, July-
581 September, 3235.

- 582 7. Depoorter, M. A., Bamber, J. L., Griggs, J. A., Lenaerts, J. T. M., Ligtenberg, S. R. M.,
583 van den Broeke, M. R., & Moholdt, G. (2013). Calving fluxes and basal melt rates of
584 Antarctic ice shelves. *Nature*, 502(7469), 89-92.
- 585 8. Domack, E., Duran, D., Leventer, A., Ishman, S., Doane, S., McCallum, S., ... & Prentice,
586 M. (2005). Stability of the Larsen B ice shelf on the Antarctic Peninsula during the
587 Holocene epoch. *Nature*, 436(7051), 681-685.
- 588 9. Fretwell, P., Pritchard, H. D., Vaughan, D. G., Bamber, J. L., Barrand, N. E., Bell, R., ...
589 & Fujita, S. (2013). Bedmap2: improved ice bed, surface and thickness datasets for
590 Antarctica. *Cryosphere*, 7(1).
- 591 10. Frezzotti, M., Cimbelli, A., & Ferrigno, J. G. (1998). Ice-front change and iceberg
592 behaviour along Oates and George V Coasts, Antarctica, 1912-96. *Annals of Glaciology*,
593 27, 643-650.
- 594 11. Fricker, H. A., Young, N. W., Allison, I., & Coleman, R. (2002). Iceberg calving from
595 the Amery ice shelf, East Antarctica. *Annals of Glaciology*, 34(1), 241-246.
- 596 12. Griggs, J. A., & Bamber, J. L. (2011). Antarctic ice-shelf thickness from satellite radar
597 altimetry. *Journal of Glaciology*, 57(203), 485-498.
- 598 13. Holland, P. R., Corr, H. F., Pritchard, H. D., Vaughan, D. G., Arthern, R. J., Jenkins, A.,
599 & Tedesco, M. (2011). The air content of Larsen ice shelf. *Geophysical Research Letters*,
600 38(10).
- 601 14. Jakobsson, M., Anderson, J. B., Nitsche, F. O., Dowdeswell, J. A., Gyllencreutz, R.,
602 Kirchner, N., ... & Majewski, W. (2011). Geological record of ice shelf break-up and
603 grounding line retreat, Pine Island Bay, West Antarctica. *Geology*, 39(7), 691-694.

- 604 15. Jenkins, A., Dutrieux, P., Jacobs, S. S., McPhail, S. D., Perrett, J. R., Webb, A. T., &
605 White, D. (2010). Observations beneath Pine Island Glacier in West Antarctica and
606 implications for its retreat. *Nature Geoscience*, 3(7), 468-472.
- 607 16. Joughin, I., & Alley, R. B. (2011). Stability of the West Antarctic ice sheet in a warming
608 world. *Nature Geoscience*, 4(8), 506-513.
- 609 17. Kusahara, K., Hasumi, H. & Williams, G. D. (2011), Impact of the Mertz Glacier Tongue
610 calving on dense water formation and export. *Nature communications*, 2, 159.
- 611 18. Kern, S., & Spreen, G. (2015), Uncertainties in Antarctic sea-ice thickness retrieval from
612 ICESat. *Annals of Glaciology*, 56(69), 107.
- 613 19. Kwok, R. Cunningham, G. F., Zwally, H. J., & Yi, D. (2007). Ice, Cloud, and land
614 Elevation Satellite (ICESat) over Arctic sea ice: retrieval of freeboard. *Journal of*
615 *Geophysical Research*, 112, C12013, doi:10.1029/2006JC003978.
- 616 20. Legresy, B., Wendt, A., Tabacco, I. E., Remy, F., & Dietrich, R. (2004). Influence of
617 tides and tidal current on Mertz Glacier, Antarctica. *Journal of Glaciology*, 50(170), 427-
618 435.
- 619 21. Legresy, B., N. Young, L. Lescarmonier, R. Coleman, R. Massom, B. Giles, A. Fraser, R.
620 Warener, B. Galton-Fenzi, L. Testut, M. Houssais and G. Masse (2010), CRAC!!! in the
621 Mertz Glacier, Antarctica.
622 [http://www.antarctica.gov.au/__data/assets/pdf_file/0004/22549/ml_402353967939815_](http://www.antarctica.gov.au/__data/assets/pdf_file/0004/22549/ml_402353967939815_mertz_final_100226.pdf)
623 [mertz_final_100226.pdf](http://www.antarctica.gov.au/__data/assets/pdf_file/0004/22549/ml_402353967939815_mertz_final_100226.pdf)
- 624 22. Lescarmonier, L., Legrésy, B., Coleman, R., Perosanz, F., Mayet, C., & Testut, L. (2012).
625 Vibrations of Mertz glacier ice tongue, East Antarctica. *Journal of Glaciology*, 58(210),
626 665-676.

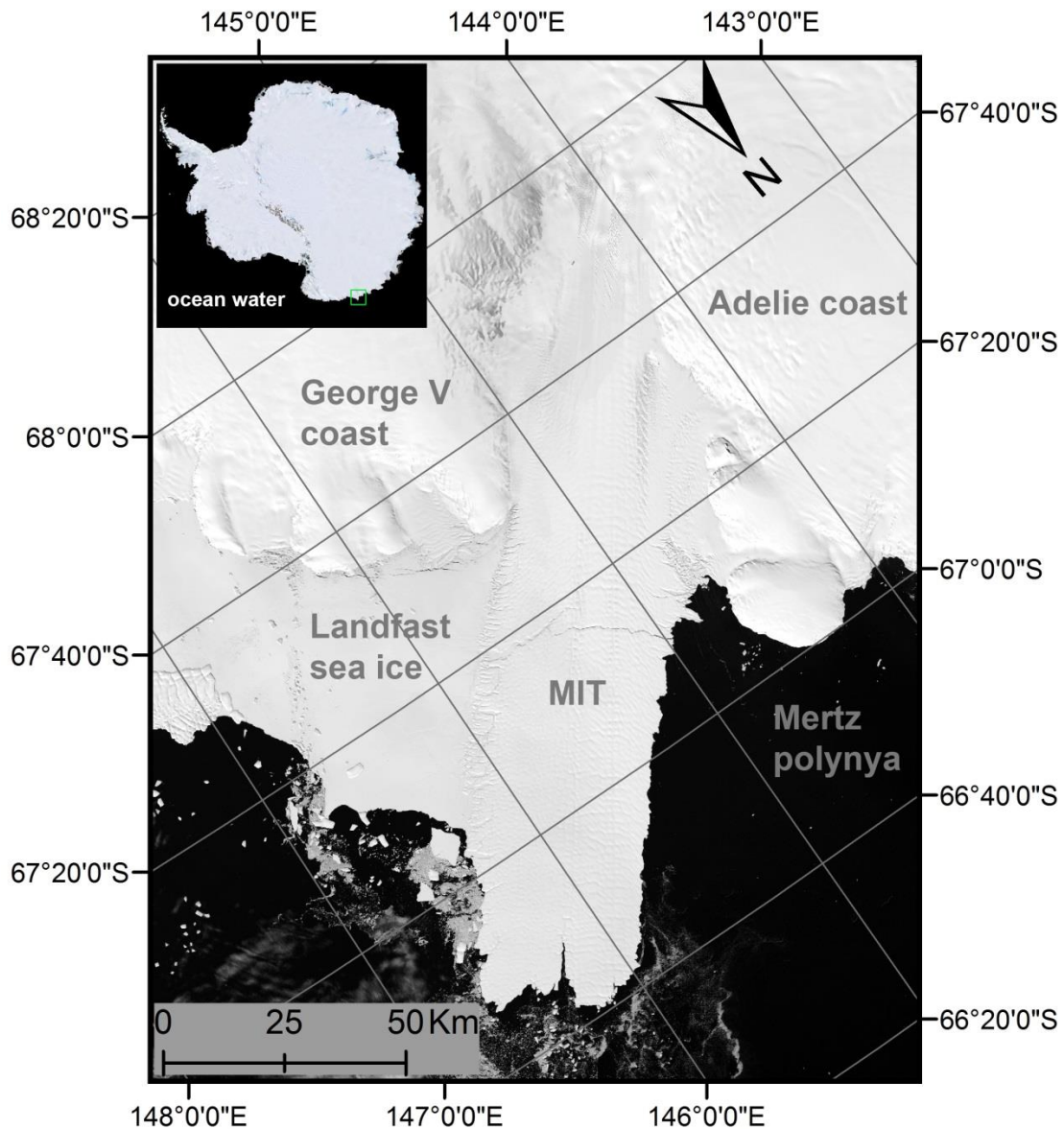
- 627 23. Ligtenberg, S. R. M., Heilsen, M. M., & van de Broeke, M. R. (2011). An improved
628 semi-empirical model for the densification of Antarctic firn. *The Cryosphere*, 5(4), 809-
629 819.
- 630 24. Ligtenberg, S., Kuipers Munneke, P., & Van Den Broeke, M. R. (2014). Present and
631 future variations in Antarctic firn air content. *The Cryosphere*, 8(5), 1711-1723.
- 632 25. Massom, R. A. (2003). Recent iceberg calving events in the Ninnis Glacier region, East
633 Antarctica. *Antarctic Science*, 15(02), 303-313.
- 634 26. Massom, R. A., Giles, A. B., Fricker, H. A., Warner, R. C., Legr ́sy, B., Hyland, G.,
635 Young, N., & Fraser, A. D. (2010). Examining the interaction between multi-year
636 landfast sea ice and the Mertz Glacier Tongue, East Antarctica: Another factor in ice
637 sheet stability? *Journal of Geophysical Research*, 115, C12027,
638 doi:10.1029/2009JC006083.
- 639 27. Massom, R. A., Giles, A. B., Warner, R. C., Fricker, H. A., Legr ́sy, B., Hyland, G., ... &
640 Young, N. (2015). External influences on the Mertz Glacier Tongue (East Antarctica) in
641 the decade leading up to its calving in 2010. *Journal of Geophysical Research: Earth*
642 *Surface*, 120(3), 490-506.
- 643 28. Pavlis, N. K., Holmes S. A., Kenyon, S. C., & Factor, J. K. (2012). The development and
644 evaluation of the Earth Gravitational Model 2008 (EGM2008), *Journal of Geophysical*
645 *Research*. 117, B04406, doi:10.1029/2011JB008916.
- 646 29. Porter-Smith, R. (2003). Bathymetry of the George Vth Land shelf and slope. *Deep Sea*
647 *Research Part II: Topical Studies in Oceanography*, 50(8), 1337-1341.

- 648 30. Pritchard, H. D., Ligtenberg, S. R. M., Fricker, H. A., Vaughan, D. G., Van den Broeke,
649 M. R., & Padman, L. (2012). Antarctic ice-sheet loss driven by basal melting of ice
650 shelves. *Nature*, 484(7395), 502-505.
- 651 31. Rignot, E., Mouginot, J. & Scheuchl, B. (2011), Ice flow of the Antarctic ice sheet.
652 *Science*, 333(6048), 1427-1430.
- 653 32. Rignot, E., & Jacobs, S. S. (2002). Rapid bottom melting widespread near Antarctic ice
654 sheet grounding lines. *Science*, 296(5575), 2020-2023.
- 655 33. Scambos, T. Hulbe, A., C. & Fahnestock, M. A. (2003). Climate-induced ice shelf
656 disintegration in the Antarctic Peninsula. *Antarctic Research Series*, 79, 79-92.
- 657 34. Scambos, T. Hulbe, A., C. Fahnestock, M. A. & Bohlander, J. (2000). The link between
658 climate warming and breakup of ice shelves in the Antarctic Peninsula. *Journal of*
659 *Glaciology*, 46(154), 516-530.
- 660 35. Shepherd, A., Wingham, D., Payne, T., & Skvarca, P. (2003). Larsen Ice Shelf has
661 progressively thinned. *Science*, 302(5646), 856-859.
- 662 36. Smith, K. L., Robison, B. H., Helly, J. J., Kaufmann, R. S., Ruhl, H. A., Shaw, T. J., ... &
663 Vernet, M. (2007). Free-drifting icebergs: hot spots of chemical and biological
664 enrichment in the Weddell Sea. *Science*, 317(5837), 478-482.
- 665 37. Smith, K. L. (2011). Free-drifting icebergs in the Southern Ocean: an overview. *Deep Sea*
666 *Research Part II: Topical Studies in Oceanography*, 58(11), 1277-1284.
- 667 38. Tamura, T., Williams, G. D., Fraser, A. D. & Ohshima, K. I. (2012). Potential regime
668 shift in decreased sea ice production after the Mertz Glacier calving, *Nature*
669 *communications*, 3, 826.

- 670 39. Tchernia, P. A. U. L., & Jeannin, P. F. (1984). Circulation in Antarctic waters as revealed
671 by iceberg tracks 1972–1983. *Polar Rec*, 22(138), 263-269.
- 672 40. Van de Berg, W. J., Van den Broeke, M. R., Reijmer, C. H., & Van Meijgaard, E. (2005).
673 Characteristics of the Antarctic surface mass balance, 1958–2002, using a regional
674 atmospheric climate model. *Annals of glaciology*, 41(1), 97-104.
- 675 41. Van de Berg, W. J., Van den Broeke, M. R., Reijmer, C. H., & Van Meijgaard, E. (2006).
676 Reassessment of the Antarctic surface mass balance using calibrated output of a regional
677 atmospheric climate model. *Journal of Geophysical Research: Atmospheres* (1984–2012),
678 111(D11).
- 679 42. Van den Broeke, M. (2008). Depth and density of the Antarctic firn layer. *Arctic,*
680 *Antarctic, and Alpine Research*, 40(2), 432-438.
- 681 43. Wang, X.W., Cheng, X., Gong, P., Huang, H. B., Li Z., & Li, X. W. (2011). Earth
682 Science Applications of ICESat/GLAS: a Review. *International Journal of Remote*
683 *Sensing*, 32, 23, 8837-8864, doi: 10.1080/01431161.2010.547533
- 684 44. Wang, X.W., Cheng, X., Gong, P., Shum, C. K., Holland, D.M., & Li, X.W. (2014).
685 Freeboard and mass extraction of the disintegrated Mertz Ice Tongue with remote sensing
686 and altimetry data. *Remote Sensing of Environment*, 144, 1-10.
- 687 45. Wang, X.W. (2014). Mertz ice tongue evolutions from satellite observed data,
688 Postdoctoral Research Report, College of Global Change and Earth System Science,
689 Beijing Normal University, China. doi: 10.13140/2.1.1006.1603
- 690 46. Wang, X., Cheng, X., Li, Z., Huang, H., Niu, Z., Li, X., & Gong, P. (2012). Lake water
691 footprint identification from time-series ICESat/GLAS data. *Geoscience and Remote*
692 *Sensing Letters, IEEE*, 9(3), 333-337.

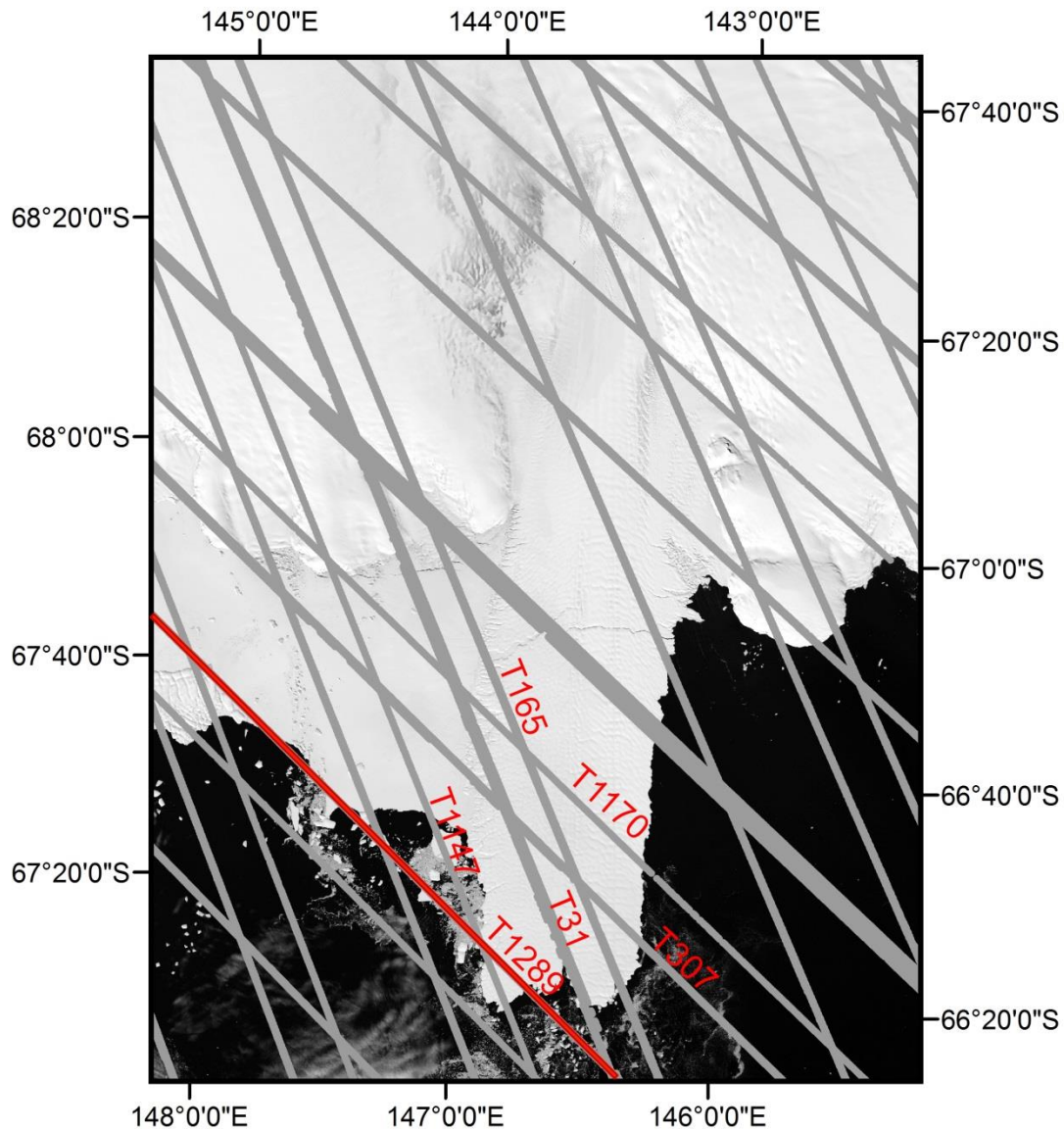
- 693 47. Wang, X., Gong, P., Zhao, Y., Xu, Y., Cheng, X., Niu, Z., ... & Li, X. (2013). Water-
694 level changes in China's large lakes determined from ICESat/GLAS data. *Remote Sensing*
695 *of Environment*, 132, 131-144.
- 696 48. Woodworth-Lynas, C. M. T., Josenhans, H. W., Barrie, J. V., Lewis, C. F. M., & Parrott,
697 D. R. (1991). The physical processes of seabed disturbance during iceberg grounding and
698 scouring. *Continental Shelf Research*, 11(8), 939-961.
- 699 49. Yi, D., Zwally, H.J., & Robbins, J. (2011). ICESat observations of seasonal and
700 interannual variations of sea-ice freeboard and estimated thickness in the Weddell Sea,
701 Antarctica (2003-2009). *Annals of Glaciology*, 52(57), 43-51.
- 702 50. Zwally, H. J., Schutz, B., Abdalati, W., Abshire, J., Bentley, C., Brenner, A., Buftona, J.,
703 Deziouf, J., Hancocka, D., Hardinga, D., Herringg, T., Minsterh, B., Quinng, K., Palmi,
704 S., Spinhirnea, J., & Thomasj, R. (2002). ICESat's laser measurements of polar ice,
705 atmosphere, ocean, and land. *Journal of Geodynamics*, 34, 405-445.
- 706 51. Zwally, H. J., Yi, D., Kwok, R., & Zhao, Y. (2008). ICESat measurements of sea ice
707 freeboard and estimates of sea ice thickness in the Weddell Sea. *Journal of Geophysical*
708 *Research*, 113, C02S15, doi:10.1029/2007JC004284.
- 709

Figures



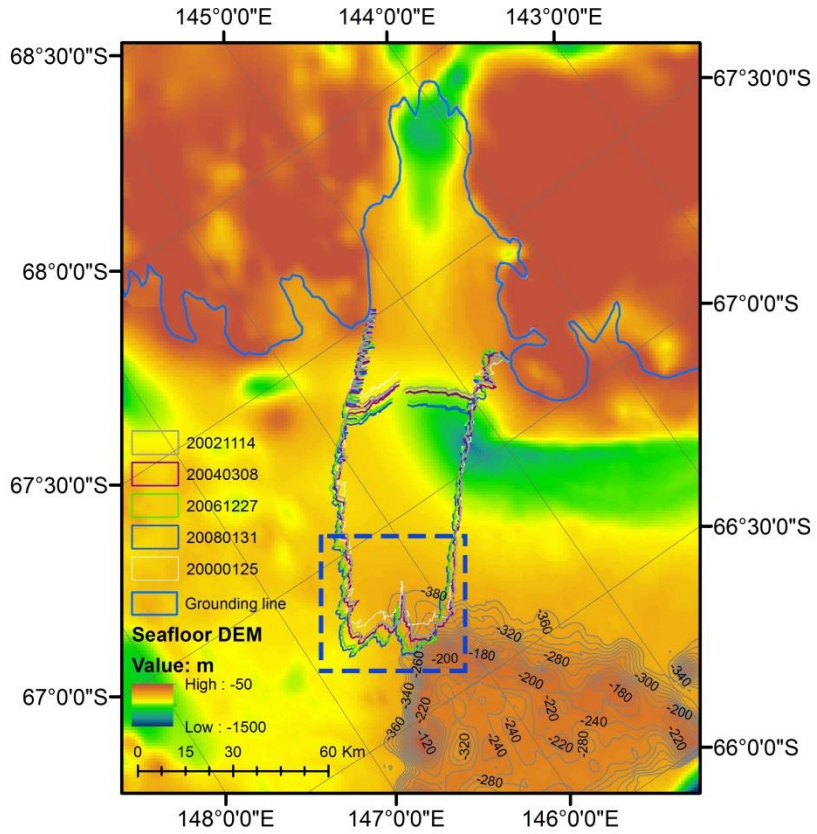
711

712 **Figure 1.** Mertz Ice Tongue (MIT), East Antarctica. Landfast sea ice is attached to the east flank
 713 of the MIT and the Mertz Polynya is to the west. The background image is from band 4 Landsat
 714 7, captured on February 2, 2003. The green square found in the upper left inset indicates the
 715 location of the MIT in East Antarctica. A polar stereographic projection with -71 °S as standard
 716 latitude is used.



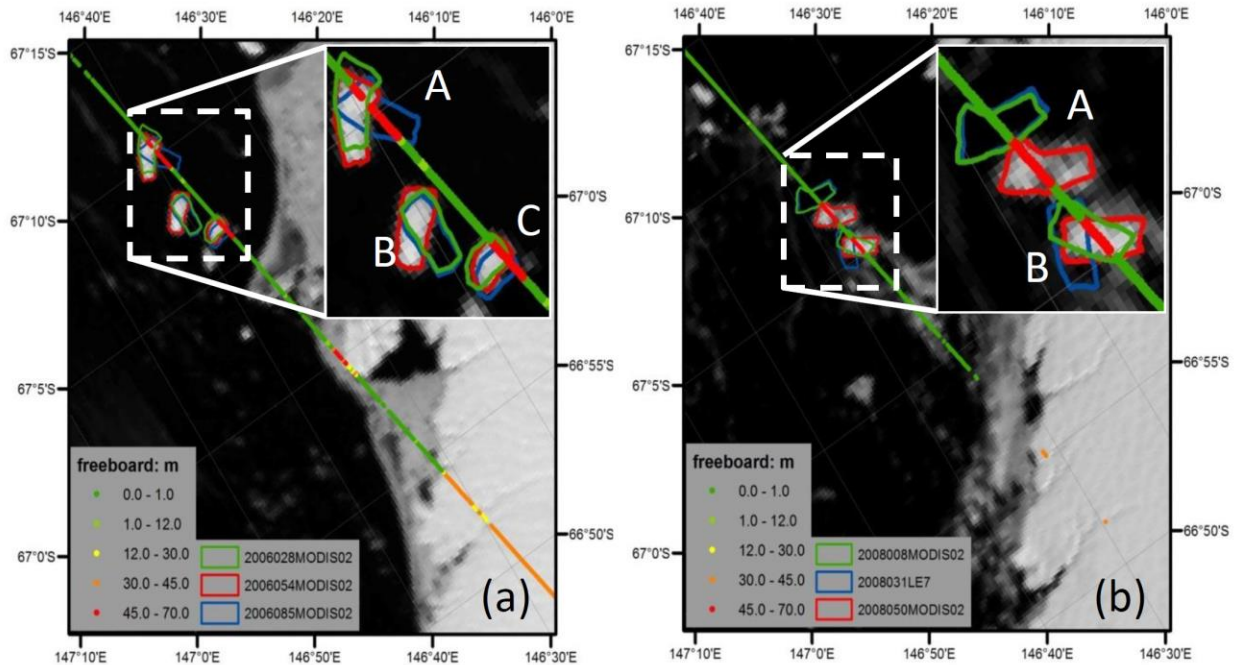
718

719 **Figure 2.** Spatial distribution of ICESat/GLAS data from 2003 to 2009 covering the Mertz
 720 region. Ground tracks of ICESat/GLAS are indicated with gray lines. Track 1289 (T1289) is
 721 highlighted in red as is used in Fig. 4. The background image is from band 4 Landsat 7, captured
 722 on February 2, 2003. A polar stereographic projection with -71 °S as standard latitude is used.



723

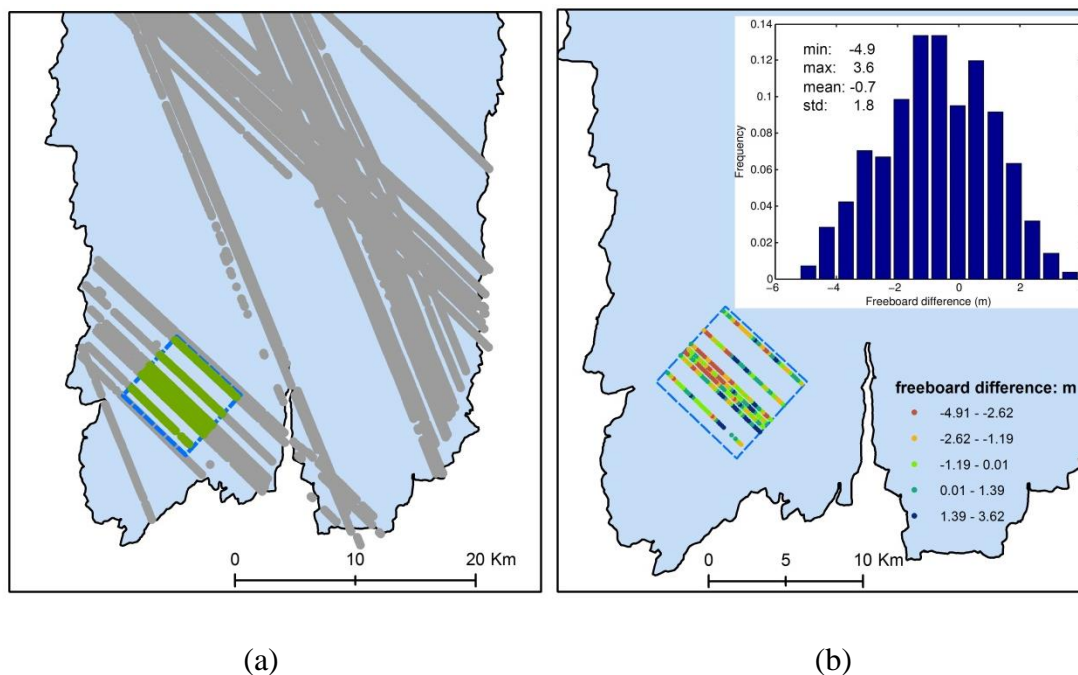
724 **Figure 3.** Seafloor topography from bathymetry around Mertz region and outlines of the MIT
 725 from 2002 to 2008. The outlines of the MIT in different years are marked with different colored
 726 polygons. The shallow Mertz Bank is located in the lower right (northeast). The blue inset box
 727 corresponds to location of Fig, 6 and 7. The bathymetry measurement profile can be found from
 728 S-Fig, 1.



729

730 **Figure 4.** Freeboard extracted from Track 1289, ICESat/GLAS, the location of which can be
 731 found in Fig. 2 and S-Fig. 1. (a) and (b) show the freeboard extracted from ICESat/GLAS on
 732 February 23, 2006 (2006054) and February 18, 2008 (2008049) respectively. In each image,
 733 positions of three icebergs (with name labeled as ‘A’, ‘B’ and ‘C’) closest to ICESat/GLAS
 734 observation time are plotted with green, red and blue polygons respectively. The dates are
 735 indicated with seven numbers (yyyyddd) in legend. ‘yyyyddd’ stands for day ‘ddd’ in year
 736 ‘yyyy’. ‘MODIS02’ and ‘LE7’ indicate that the image used to extract iceberg outline is from
 737 MODIS and Landsat 7 ETM+, respectively.

738



740

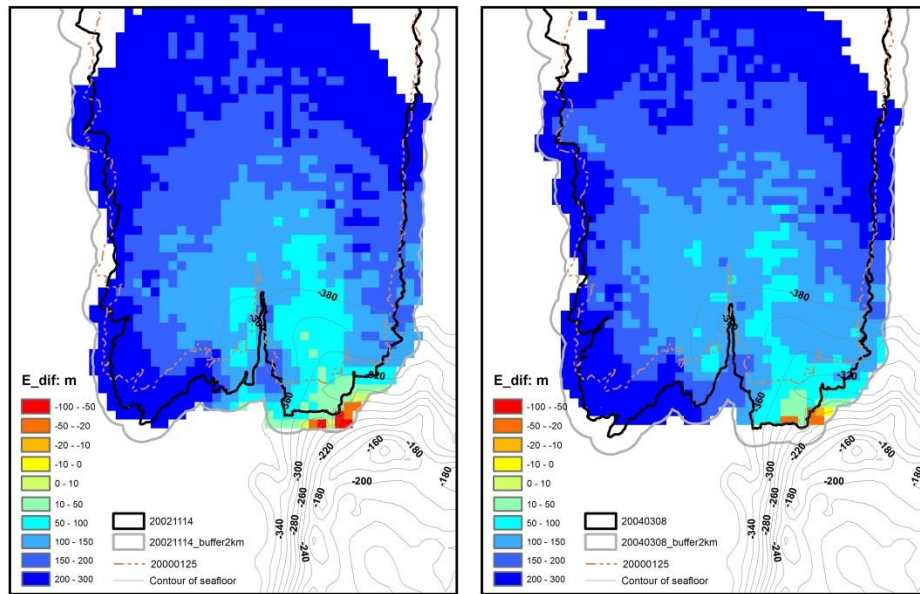
741

742 **Figure 5.** Evaluation of kriging interpolation method over the MIT using freeboard data derived
 743 from ICESat/GLAS. (a) is freeboard data derived from ICESat/GLAS after relocation over the
 744 MIT. Gray dots indicate ICESat/GLAS used for interpolation using kriging method. The blue
 745 dashed square indicates the region used to investigate interpolation accuracy of kriging method,
 746 about 7 km \times 7 km. Inside of the square, freeboard data marked with green dots are used to check
 747 the accuracy of freeboard interpolated with kriging. (b) is the freeboard comparison result
 748 derived by subtracting krigged freeboard from freeboard derived from ICESat/GLAS. The spatial
 749 distribution and the histogram of freeboard difference is shown in the lower left and upper right
 750 respectively. The black polygon filled with light blue shows the boundary of MIT on November
 751 14, 2002.

752

753

754

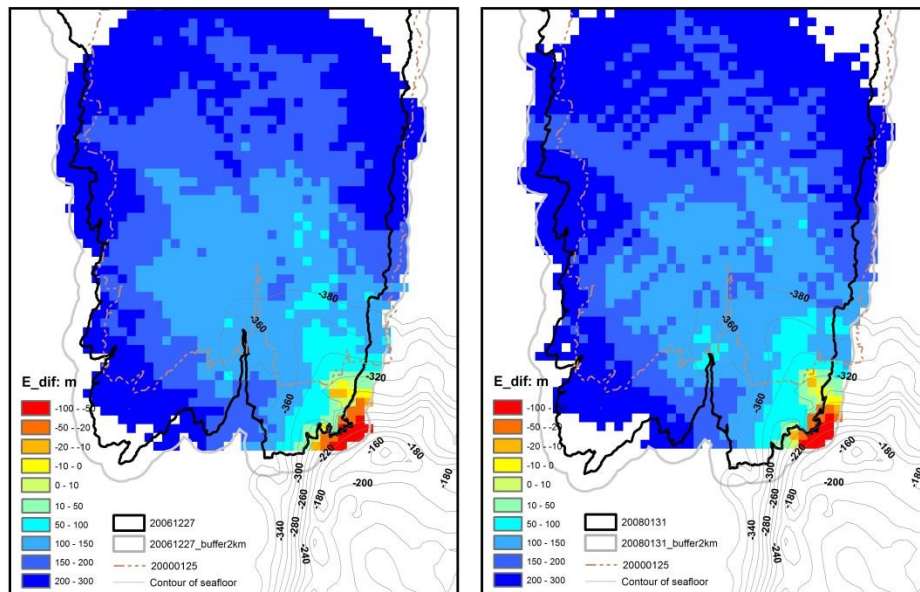


755

756

(a)

(b)



757

758

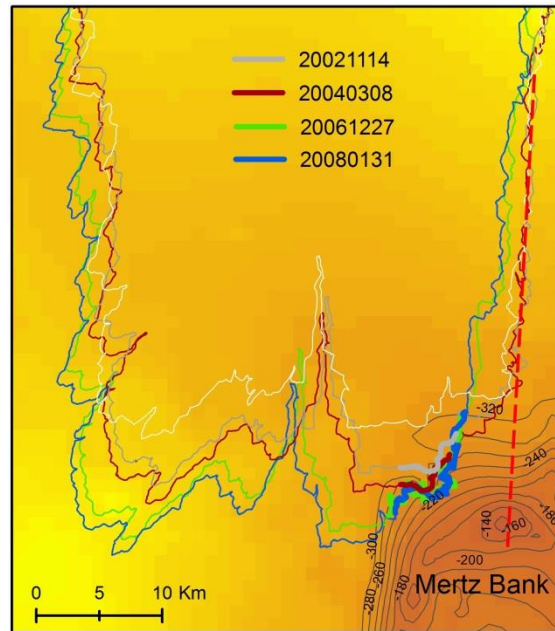
(c)

(d)

759 **Figure 6.** Elevation difference of Mertz ice bottom and seafloor topography. (a), (b), (c) and (d)
760 correspond to elevation difference assuming hydrostatic equilibrium under the minimum sea
761 surface height -3.35 m on November 14, 2002 , March 8, 2004, December 27, 2006, and January

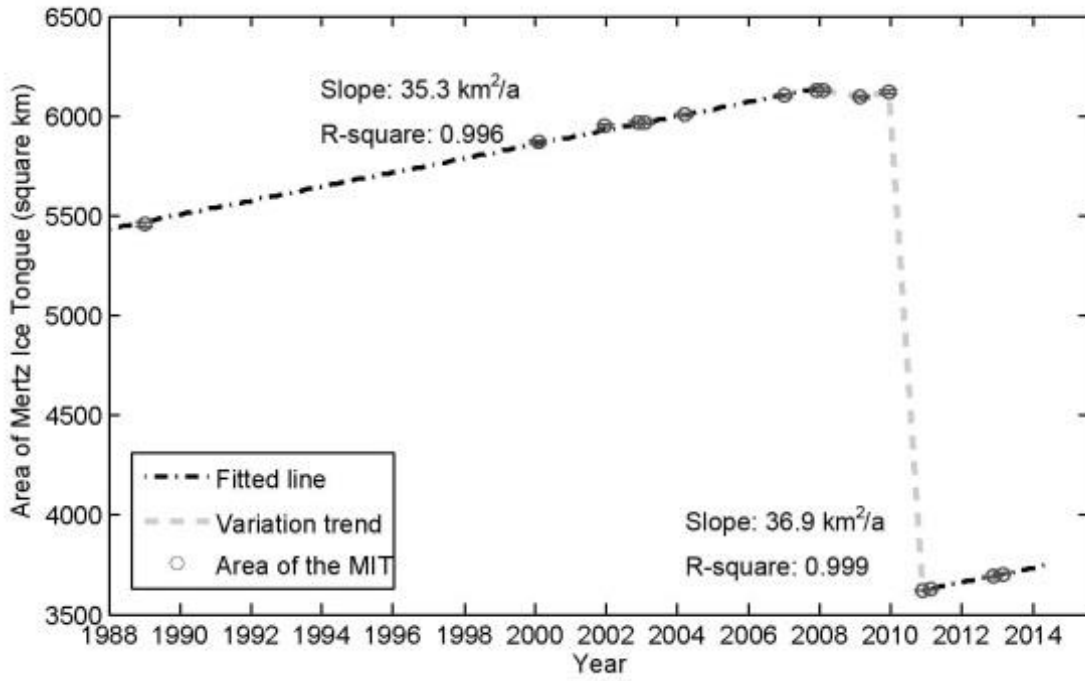
762 31, 2008, respectively. The contours in the lower right indicate seafloor topography (unit: m) of
763 the Mertz Bank with an interval of 20 m. The solid black line indicates the boundary of the MIT
764 and the thick gray line outlines a buffer region of the boundary with 2 km as buffer radius. The
765 dashed line indicates the shape of the MIT on January 25, 2000, which is used to identify the
766 bathymetry gap under the ice tongue. In the legend, negative values mean that ice bottom is
767 lower than the seafloor, which of course is impossible. Therefore, the initial assumption of a
768 floating ice tongue was incorrect in those locations (yellow to red colors), and the ice was
769 grounded. Regions with more negative values indicate more heavily grounding inside of the MIT
770 or more heavily grounding potential in the buffer region.

771



772

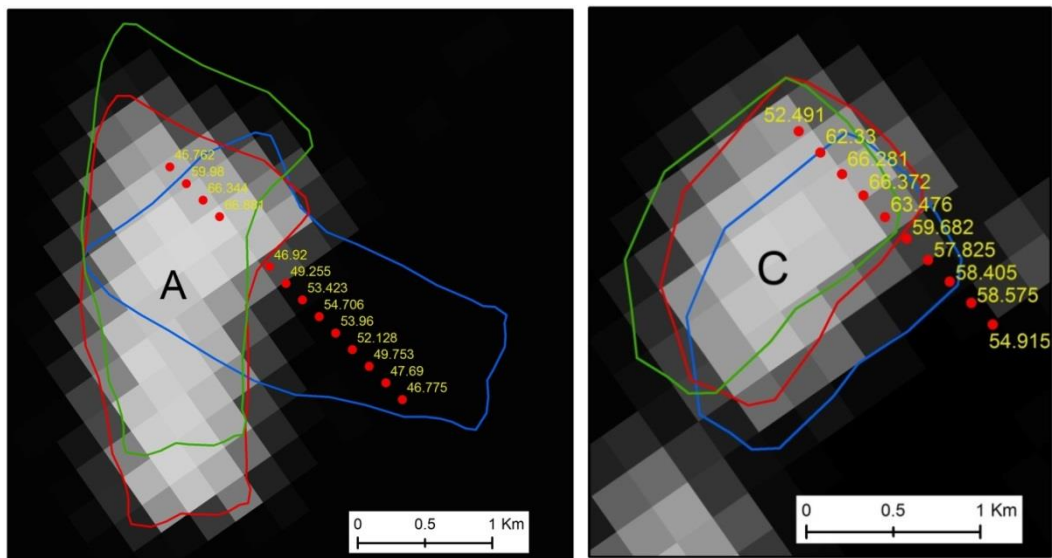
773 **Figure 7.** Digital Elevation Map (DEM) of seafloor around Mertz and grounding section of the
774 boundaries extracted from 2002 to 2008. Grounding section of MIT boundary in 2002, 2004,
775 2006 and 2008 is marked with thick gray, purple, green and blue polylines respectively and MIT
776 boundaries are indicated with polygons with the same legend as Fig. 3. Additionally, MIT
777 boundary in 2000 indicated with white polygon is used to show the different quality of seafloor
778 DEM. Inside of this polygon no bathymetry data was collected or used. The dashed red line
779 indicates the 'extension line' of the west flank of MIT on November 14, 2002, passing the
780 shallowest region of the Mertz Bank (about -140 m).



781

782 **Figure 8.** Time series of area change of the MIT. The area covers the entire ice tongue, to the
 783 grounding line as indicated with thick blue line in Fig. 3. The area is extracted from Landsat
 784 images from 1988 to 2013.

785

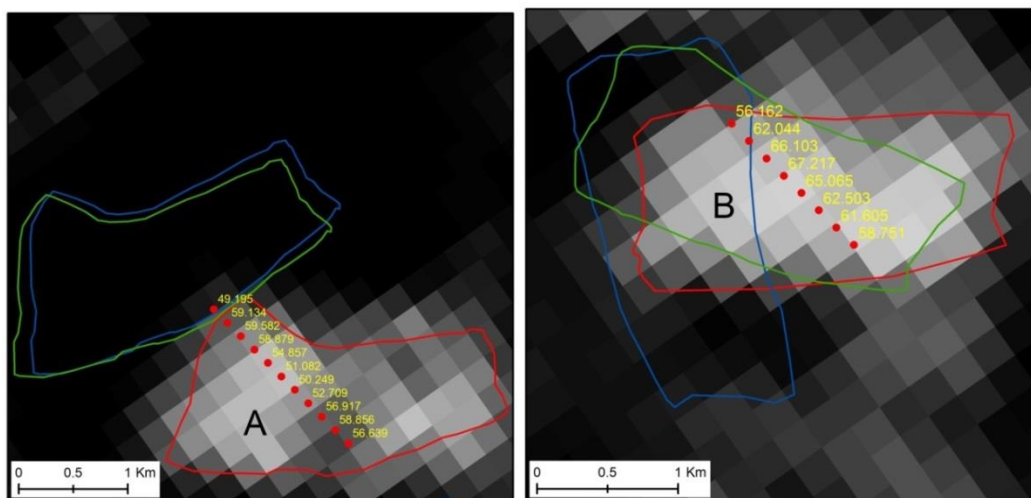


787

788

(a)

(b)



789

790

(c)

(d)

791 **Figure 9.** Freeboard extraction results from ICESat/GLAS for icebergs ‘A’, ‘B’ and ‘C’ in 2006

792 and 2008 respectively. (a) and (b) correspond to freeboard measurements from ‘A’ and ‘C’

793 respectively on February 23, 2006 (2006054), with background image from MODIS captured on

794 2006054. (c) and (d) correspond to freeboard measurements from ‘A’ and ‘B’ respectively on

795 February 18, 2008 (2008049), with background image from MODIS captured on 2008050. The

796 location of each iceberg in different observation time is indicated with different colored polygons,
797 the legend of which is the same as what is used in Fig. 4. Inside of each sub-figure, different
798 icebergs are marked with capital characters 'A', 'B' and 'C' respectively and iceberg freeboard
799 results in unit of meter are marked in yellow.

800

801

Tables

802 **Table 1.** Statistics of the three icebergs used to inverse FAC with least-square method. Icebergs
 803 ‘A’, ‘B’ and ‘C’ are the same as what are used in Fig. 4 and 9. Measurements from icebergs ‘A’
 804 and ‘C’ in February 2006 are used to derive FAC with least-squares method. Icebergs ‘A’ and ‘B’
 805 in 2008 are used for validation.

| Icebergs | date | Latitude ($^{\circ}$) | Longitude ($^{\circ}$) | Freeboard (m) | Seafloor (m) | Sea level (m) | ε (m) | E_{dif} (m) |
|----------|-----------------|----------------------------|-----------------------------|------------------|-----------------|------------------|----------------------|------------------|
| A | Feb 23, 2006 | -67.1737 | 146.6595 | 66.88 | -528.48 | -1.92 | 0.89 | |
| | | -67.1752 | 146.6604 | 66.34 | -527.01 | -1.92 | 1.30 | |
| C | Feb 23, 2006 | -67.1085 | 146.6247 | 66.37 | -505.84 | -1.92 | -1.25 | |
| | | -67.1100 | 146.6255 | 66.28 | -507.08 | -1.92 | -1.01 | |
| A | Feb 18, 2008 | -67.1194 | 146.6303 | 58.88 | -522.52 | -2.08 | | 69.14 |
| | | -67.1209 | 146.6311 | 59.58 | -524.16 | -2.08 | | 64.88 |
| B | Feb 18, 2008 | -67.0906 | 146.6151 | 67.22 | -500.92 | -2.08 | | -22.45 |
| | | -67.0921 | 146.6159 | 66.10 | -500.47 | -2.08 | | -13.55 |

806

807 **Table 2.** Statistics of grounding grids inside or grounding potentials outside of the Mertz Ice
808 Tongue (MIT) (‘I’: inside of thick black line, Fig. 6; Number in brackets indicates how many
809 grids are located inside of the 2000 Mertz boundary; ‘O’: between the black and gray lines, Fig.
810 6) on November 14, 2002, March 8, 2004, December 27, 2006 and January 31, 2008 respectively.
811 Each grid covers an area of 1 km². The Mean, Minimum and Standard deviation is calculated
812 without considering those fallen inside of the 2000 Mertz boundary, but only those having
813 elevation difference less than 46 m and out of 2000 Mertz boundary.

814

| Elevation difference (subtracting seafloor from ice bottom) | 2002-11-14 | | 2004-03-08 | | 2006-12-27 | | 2008-01-31 | |
|---|------------|-------|------------|-------|------------|--------|------------|--------|
| | I | O | I | O | I | O | I | O |
| 23-46 (m) | 9(3) | 10(0) | 6(0) | 3(0) | 10(1) | 1(0) | 10(3) | 5(0) |
| 0-23 (m) | 2(0) | 6(0) | 1(0) | 1(0) | 9(0) | 2(0) | 4(0) | 2(0) |
| <0 (m) | 0(0) | 8(0) | 2(0) | 5(0) | 7(0) | 21(0) | 6(0) | 18(0) |
| Mean (m) | 28.8 | 9.8 | 15.8 | -1.1 | 10.9 | -41.9 | 12.3 | -31.0 |
| Minimum (m) | 11.9 | -81.5 | -46.0 | -44.5 | -52.3 | -102.8 | -34.8 | -103.0 |
| Standard deviation (m) | 9.2 | 36.8 | 29.6 | 31.4 | 24.7 | 37.6 | 27.3 | 38.0 |
| Number of grids | 8 | 24 | 9 | 9 | 25 | 24 | 17 | 25 |

815

816 **Table 3.** Statistics of grounding outlines of the MIT as shown with thick polylines in Fig. 7 on
 817 November 14, 2002, March 8, 2004, December 27, 2006 and January 31, 2008 respectively

| | 2002-11-14 | 2004-03-08 | 2006-12-27 | 2008-01-31 |
|--------------------|--------------------------|--------------------------|--------------------------|--------------------------|
| Start location (°) | 146.124 °E, 66.696 °S | 146.155 °E, 66.681 °S | 146.093 °E, 66.700 °S | 146.088 °E, 66.699 °S |
| End location (°) | 146.240 °E, 66.693 °S | 146.256 °E, 66.683 °S | 146.304 °E, 66.669 °S | 146.292 °E, 66.668 °S |
| Perimeter (km) | 7.0 | 6.4 | 24.7 | 20.9 |

818